THE JOURNAL OF PHYSICAL CHEMISTRY C

Article

pubs.acs.org/JPCC

Molecular Dynamics Simulation of Diffusion and Electrical Conductivity in Montmorillonite Interlayers

J. A. Greathouse,*[,†] R. T. Cygan,[†] J. T. Fredrich,[‡] and G. R. Jerauld[‡]

[†]Sandia National Laboratories, Albuquerque, New Mexico 87185-0754, United States

[‡]BP America, 501 Westlake Park Boulevard, Houston, Texas 77024, United States

ABSTRACT: The diffusion of water and ions in the interlayer region of smectite clay minerals represents a direct probe of the type and strength of clay−fluid interactions. Interlayer diffusion also represents an important link between molecular simulation and macroscopic experiments. Here we use molecular dynamics simulation to investigate trends in cation and water diffusion in montmorillonite interlayers, looking specifically at the effects of layer charge, interlayer cation and cation charge (sodium or calcium), water content, and temperature. For Na-montmorillonite, the largest increase in ion and water diffusion coefficients occurs between the one-layer and two-layer hydrates, corresponding to the transition from inner-sphere to outer-sphere surface complexes. Calculated activation energies for ion and water diffusion in Na-montmorillonite are similar to each other and to the water hydrogen bond energy, suggesting the breaking of water−water and water−clay hydrogen bonds as a likely mechanism for interlayer diffusion. A comparison of interlayer diffusion with that of bulk electrolyte solutions reveals a clear trend of decreasing diffusion coefficient with increasing electrolyte concentration, and in most cases the interlayer diffusion results are nearly coincident with the corresponding bulk solutions. Trends in electrical conductivities computed from the ion diffusion coefficients are also compared.

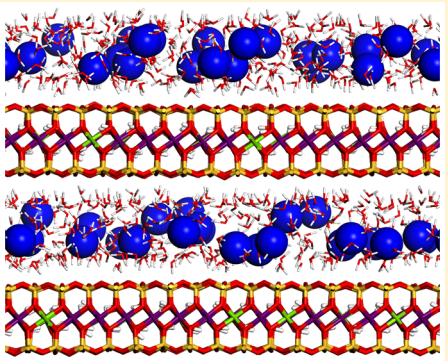

INTRODUCTION

Diffusion of water molecules and cations in the interlayer of swelling clay minerals, known as the smectite group (and which includes montmorillonite), is a critical process that controls ion exchange and adsorptive properties important to many environmental, industrial, petroleum, and related engineering systems.[1−6] The nanoconfinement of water and cations in the interlayer region of smectite minerals offers a unique opportunity to examine the influence of water content, cation charge, and the influence of clay surfaces on the transport properties of interlayer species. These molecular properties, combined with the low permeability of clay-rich rocks such as bentonite, underscore the use of clays and clay minerals as adsorptive backfill materials for the safe isolation of high-level radioactive waste in geological waste repositories.[7−10] Similarly, such natural and modified materials are often used for the remediation of chemical waste spills to prevent the spread of contaminants into the greater environment.[11−13] Clays are an important mineral in many subsurface environments, and understanding their properties is important for many energy applications.

Recent advances in computational chemistry and molecular dynamics (MD) methods have led to new understanding of clay interlayer structures and the diffusion rates of various interlayer cations and water.[14−17] For example, it is now widely accepted that water properties, including diffusion rates, are affected by nanoconfinement. The swelling of a clay interlayer from a collapsed structure with no water to one, two, and three water-layer hydrates with layer thicknesses of about 3 to 6 to 9 Å is primarily dependent on relative humidity and clay surface charge.[18,19] MD studies have successfully investigated the molecular mechanism of smectite swelling and determined the distribution of cations and water molecules within the interlayer.[20−25] Furthermore, the use of molecular simulation to derive diffusion rates of interlayer species in clay minerals provides an important link to macroscopic experiments and field measurements. Simulation-derived diffusion rates can be used to evaluate time and distance constraints for geochemical processes involving chemical species within clay particles and nanopore environments. Additionally, diffusion of charged species (cations) in the clay interlayer or in clay-dominated nanopores is fundamentally equivalent to electrical conductivity, which is itself a common probe of fluid composition and behavior used in petroleum drilling operations, oil exploration, reservoir characterization, pipeline flow, and disposition of hazardous materials.[26−29]

In this work we use MD simulations to compute diffusion coefficients of ions and water molecules confined to the interlayer regions of bulk clay minerals. We compare the effects of cation hydration enthalpy (Na^+ vs Ca^{2+}), layer charge, water content, and temperature for conditions expected in various technical applications. Rather than comparing interlayer

Received: November 5, 2015
Revised: December 23, 2015
Published: January 20, 2016

DOI: 10.1021/acs.jpcc.5b10851
J. Phys. Chem. C 2016, 120, 1640−1649

Table 1. Composition of Clay Simulation Systems

layer charge (e · unit cell^{-1})	counterion	T (K)	water layers	$d(001)$ (Å)[a]	ion concentration	
					M	10^3 ppm
−0.375	Na^+	300	1W	12.49	4.6	87
			2W	15.23	2.4	45
			3W	17.54	1.7	31
		366	1W	12.63	4.4	87
			2W	15.56	2.3	45
			3W	18.15	1.6	31
	Ca^{2+}	300	1W	14.48	1.4	45
			2W	15.17	1.2	23
			3W	17.41	0.9	16
−0.750	Na^+	300	1W	12.20	10.3	160
			2W	14.79	5.2	87
			3W	17.00	3.6	60
		330	1W	12.23	10.3	160
			2W	14.89	5.2	87
			3W	17.21	3.5	60
		366	1W	12.28	10.0	160
			2W	14.99	5.0	87
			3W	17.46	3.4	60
	Ca^{2+}	300	1W	14.08	3.0	87
			2W	14.67	2.6	45
			3W	16.74	1.9	31

[a]Uncertainties in all $d(001)$ spacings were less than 0.07 Å.

diffusion coefficients with bulk water or ions at infinite dilution, results are compared to bulk solutions at equivalent concentrations as the clay interlayers. Finally, electrical conductivity values are computed from the interlayer ion diffusion coefficients, and a comparison of these conductivities relative to bulk solutions provides useful insight for the interpretation of conductivity measurements in rocks containing clays. The length scale of porosity in clay-bearing reservoir sands ranges over several orders of magnitude, from mesoscale pores hundreds of microns in dimension down to nanoscale porosity separating individual clay layers. There is an exceptionally large range of observed clay fabric and habitat due to the large range not just in clay type but, more significantly, in complex and varied diagenesis. Clay mineral interlayers and bulk solutions therefore represent the minimum and maximum porosity expected in such natural rock phases.

METHODS

Initial atomic coordinates for the smectite model were taken from a similar layer structure (muscovite) which contains interlayer potassium ions but no interlayer water molecules.[30] Removing the interlayer potassium ions and replacing all aluminum atoms in the tetrahedral sheets with silicon atoms resulted in a generic neutral structure with unit cell formula $[Si_8](Al_4)O_{20}(OH)_4$, with silicon and aluminum atoms in tetrahedral and octahedral coordination, respectively. After orthogonalization, a supercell containing 8 × 4 × 2 repeats in the x, y, and z directions was created, with approximate dimensions in the xy plane of 41 Å × 36 Å. The neutral supercell was transformed into a montmorillonite model by randomly replacing aluminum atoms in the octahedral sheet with magnesium atoms.[31] While creating the negative charge sites, care was taken to avoid nearest neighbor Mg−O−Mg interactions. Two montmorillonite models were created, corresponding to unit cell (u.c.) layer charges of −0.375 e/u.c. and −0.750 e/u.c, denoted as "low-charge" and "high-charge", respectively. After balancing the layer charge with interlayer sodium ions, unit cell formulas for the montmorillonite models were $Na_{0.375}[Si_8](Al_{3.625}Mg_{0.375})O_{20}(OH)_4$ and $Na_{0.75}[Si_8](Al_{3.25}Mg_{0.75})O_{20}(OH)_4$. Analogous Ca-montmorillonite models were created, with only half the number of calcium ions as sodium ions needed for charge balance.

Models of hydrated montmorillonites were created by expanding the interlayer regions of the anhydrous models and adding an appropriate number of water molecules to create one-layer (1W), two-layer (2W), and three-layer (3W) hydrates. The stoichiometric ratios of water molecules per unit cell (3.9, 7.9, and 11.8) are consistent with previous simulation studies of montmorillonite hydrates.[32] Counterions were initially placed in the midplane between clay layers, above (or below) negative charge sites. The remaining accessible region of the interlayer was filled with the appropriate number of water molecules in a grid pattern that avoided close contacts with counterions or siloxane surfaces. During an initial energy minimization, water molecules formed hydration shells about the counterions. Ion concentrations in the montmorillonite systems (Table 1) were calculated from the accessible volume of the interlayers. Each clay layer was assumed to have a thickness of 9.6 Å, which is equivalent to the $d(001)$ spacing of dehydrated Na-montmorillonite.[33] Therefore, for each hydrated clay model, a layer thickness of 2 × 9.6 Å was subtracted from each equilibrated cell z parameter in determining the interlayer accessible volume. Likewise, porosity values for each equilibrated system were calculated as the ratio of accessible volume to total volume. In estimating this accessible volume, the contribution from hexagonal cavities at the siloxane surfaces is indirectly included, since interlayer cations can occupy these cavities.[34] However, this volume contribution is negligible compared to the total accessible volume.

In order to compare ion and water diffusion coefficients with values from bulk solution, separate bulk solution models were created containing either 4096 or 5832 water molecules in a

DOI: 10.1021/acs.jpcc.5b10851
J. Phys. Chem. C 2016, 120, 1640−1649

cubic simulation cell for dilute and more concentrated solutions, respectively. Neutral NaCl and $CaCl_2$ solutions were created by adding the appropriate ions in stoichiometric ratios (Table 2) to achieve maximum total dissolved solids

Table 2. Composition of Bulk Simulation Systems

					solution concentration	
solution	T (K)	N_{cation}	N_{water}	L (Å)[a]	M	10^3 ppm
NaCl	300	4	4096	49.7	0.05	2
		96	5832	56.3	0.90	32
		144	5832	56.4	1.33	47
		312	5832	57.1	2.78	97
	366	4	4096	50.6	0.05	1.9
		96	5832	57.2	0.85	32
		144	5832	57.4	1.27	47
		312	5832	56.4	2.65	97
$CaCl_2$	300	4	4096	49.7	0.05	3
		48	5832	56.2	0.45	24
		64	5832	56.3	0.60	32
		96	5832	56.4	0.89	47

[a]Uncertainties in cell parameters (L) were less than 0.07 Å.

(TDS) concentrations similar to the 2W clay systems. A TDS concentration is independent of estimated volume and importantly highlights the lack of anions in the interlayer fluids. Additionally, the TDS concentration unit is common to conductivity measurements in laboratory and field experiments. These systems resulted in average cell parameters of at least 50 Å, which minimizes the dependence of system size on bulk diffusion.[35]

All interaction parameters were taken from Clayff[20] and will only be briefly described here. Clayff allows for full flexibility of clay layers and has been shown to accurately reproduce structural and spectroscopic properties of clays[20,31,36−39] as well as dynamical and energetic properties of clay interlayers and aqueous interfaces.[40−45] Other than bonded interactions required for montmorillonite hydroxyl groups and water molecules, potential energies were calculated from pairwise nonbonded (electrostatic and van der Waals) interactions. van der Waals parameters for oxygen atoms in Clayff are based on the flexible SPC water model,[46] which was also used for interlayer water molecules.

MD simulations were performed with the LAMMPS code[47] at a temperature of 300 K for all systems and at higher temperatures of 330 K and 366 K for selected systems. Short-range interactions were evaluated every 0.5 fs with a real-space cutoff of 10.0 Å. Three-dimensional periodic boundary conditions were applied, and long-range electrostatic interactions were evaluated every 1.0 fs with the particle−particle particle−mesh (PPPM) summation algorithm[48] and a precision of 1.0×10^{-4}. Model systems were thermally equilibrated using an initial 50 ps simulation in the microcanonical (particle number N, volume V, potential energy E) ensemble with velocity rescaling according to the desired temperature, followed by an additional 50 ps simulation in the NVT (canonical) ensemble, where T is the Nose−Hoover thermostat[49] temperature. A 2500 ps production simulation was then performed in the NPT (isothermal−isobaric) ensemble, with the Nose−Hoover barostat[49] pressure P set to zero. Supercell volume changes were allowed in the z direction only (x and y remained fixed at their optimized values). A snapshot of the MD-equilibrated Na-montmorillonite 3W system is shown in Figure 1.

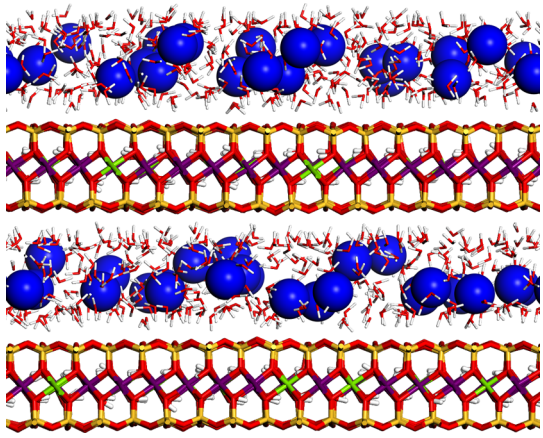

Figure 1. Snapshot of the simulation supercell for Na-montmorillonite (layer charge −0.750 e/u.c.) at 300 K. Atoms are colored as follows: Na (blue), O (red), H (white), Si (yellow), Al (purple), Mg (green).

Atomic coordinates from the final 2000 ps of NPT simulation were stored every 2.0 fs and were used for diffusion analysis. Ion and water self-diffusion coefficients (D) were calculated from the mean-square displacement (Einstein equation)[49] for interlayer (two-dimensional) diffusion parallel to the basal surface (i.e., xy plane)

$$\langle \Delta x(t)^2 + \Delta y(t)^2 \rangle = 4Dt \quad (1)$$

or three-dimensional diffusion in bulk solutions

$$\langle \Delta x(t)^2 + \Delta y(t)^2 + \Delta z(t)^2 \rangle = 6Dt \quad (2)$$

where the brackets denote an ensemble average of particle displacement (e.g., Δx) at time t. Equation 1 was applied for each ion type and all water molecules in the simulation cell, and D was calculated between 150 and 250 ps,[35] based on observations that interlayer diffusion can be overestimated if calculated over shorter times.[14] Plots of mean-square displacement versus time from similar simulations show that the linear behavior can change over time,[50] but we have minimized this problem by restarting our calculation at each data frame (2.0 fs). Errors in the slopes determined from linear least-squares analysis were approximately 0.01% and correspond to errors in D of 0.05%−0.65% for ions and 0.01%−0.10% for water.

Ion conductivities σ_i (i = Na^+ or Ca^{2+}) were then calculated using the Nernst−Einstein relationship[51]

$$\sigma_i = \frac{z_i^2 c_i F^2 D_i}{RT} \quad (3)$$

where z_i is the ion valency, c_i is the ion concentration, F is the Faraday constant, and R is the gas constant. In the above equations, units of the simulated properties (e.g., Å, fs) were converted to SI units for calculation of D ($m^2 \cdot s^{-1}$) and σ ($S \cdot m^{-1}$).

RESULTS AND DISCUSSION

Calculated diffusion coefficients and electrical conductivities from MD simulations of montmorillonite interlayers are shown in Table 3. Specific trends of these transport properties are presented graphically below, so only a brief summary is

DOI: 10.1021/acs.jpcc.5b10851
J. Phys. Chem. C 2016, 120, 1640−1649

Table 3. Ion and Water Diffusion Coefficients (10^{-10} $m^2 \cdot s^{-1}$) and Electrical Conductivities ($S \cdot m^{-1}$) from MD Simulations of Montmorillonite Interlayers

layer charge (e·unit cell^{-1})	counterion[a]	T (K)	water layers	D_{ion}	D_w	σ
−0.375	Na^+	300	1W	2.2	11.4	3.7
			2W	9.3	24.1	8.2
			3W	9.9	22.9	6.2
		366	1W	9.6	37.1	12.9
			2W	23.6	65.8	16.6
			3W	24.2	68.9	14.5
	Ca^{2+}	300	1W	1.5	18.5	3.1
			2W	3.1	20.9	5.5
			3W	4.6	20.4	5.9
−0.750	Na^+	300	1W	1.6	4.6	6.3
			2W	5.1	13.1	9.9
			3W	5.6	14.8	7.5
		330	1W	3.1	9.2	10.8
			2W	10.4	24.3	18.3
			3W	11.0	27.5	13.1
		366	1W	5.5	14.7	17.4
			2W	17.0	39.4	26.7
			3W	20.7	47.5	22.9
	Ca^{2+}	300	1W	0.6	7.0	2.8
			2W	1.2	8.6	4.8
			3W	2.2	10.6	6.2

provided here. The results confirm two expected trends: diffusion coefficients for ions (D_{ion}) and water (D_w) increase as temperature increases, and they decrease as the clay layer charge increases. Interlayer regions for low-charge models contain half the number of cations as their high-charge counterparts. The reduced ion concentration, combined with the more hydrophobic clay layers confining the interlayer fluid, result in substantially larger diffusion coefficients for the low-charge systems.

For Na-montmorillonite, D_{Na} values increase sharply by a factor of 2−4 between the 1W and 2W hydration states, while D_w values approximately double between 1W and 2W. For Ca-montmorillonite, the corresponding increase in D_{Ca} and D_w values are much smaller. In the 1W state, many sodium ions are adsorbed directly on the siloxane surface (inner-sphere surface complexes), while most calcium ions have already formed full hydration shells characteristic of bulk solution. As the 2W state forms in Na-montmorillonite, sodium ions occur as fully hydrated outer-sphere complexes, which are much more mobile than inner-sphere complexes. The increase in diffusion coefficients is much smaller between the 2W and 3W states, reflecting only an increase in accessible volume rather than different ion coordination environments. In fact, D_w values in low-charge Na- and Ca-montmorillonite actually decrease slightly between the 2W and 3W states at 300 K, indicating a similarity to bulklike behavior in both states.

Comparing diffusion coefficients in montmorillonite interlayers to published values, we first note the similarity in D_{ion} and D_w values to those from MD simulations of montmorillonites,[52] hectorites,[53,54] and saponites[16] with similar layer charge to our high-charge model. The relative increase in D values between 1W and 2W states in Na-saponite is similar to our results, but there is a much larger increase in D_{Ca} (7×) and D_w (4×) between 1W and 2W.[16] The negative layer charge in saponite exists exclusively in the tetrahedral (siloxane) sheet compared to the octahedral (alumina) substitution in our montmorillonite model. As a result, interlayer calcium ions are more strongly bound to the clay surface in the 1W state of Ca-saponite compared to Ca-montmorillonite. Additionally, MD simulations of interlayer calcium structure in Ca-hectorite also showed inner-sphere calcium surface complexes in both the 1W and 2W hydration states.[37] Diffusion results for our montmorillonite model should be generally applicable to models with tetrahedral charge, at least at higher water contents where interlayer cations are likely to be fully hydrated as in our 2W and 3W states.

Diffusion coefficients in clay interlayers are often compared to the corresponding values in bulk solution to determine the effects of interlayer confinement and layer charge on mobility. Simulation results for bulk NaCl(aq) and $CaCl_2$(aq) solutions (Table 4) correspond to infinite dilution (0.05 M) and higher parts per million (ppm) concentrations seen in the 2W states of our montmorillonite models. Specific comparisons of ion and

Table 4. Ion and Water Diffusion Coefficients (10^{-10} $m^2 \cdot s^{-1}$) and Electrical Conductivities ($S \cdot m^{-1}$) from MD Simulations of Bulk NaCl and $CaCl_2$ Solutions

		solution concentration					
solution	T (K)	M	10^3 ppm	D_{caton}[a]	D_{Cl}	D_w	σ
NaCl	300	0.05	2	15.4	22.3	32.8	0.8
		0.90	32	12.8	17.7	27.6	10.2
		1.33	47	12.3	16.9	26.0	14.5
		2.78	97	9.8	12.9	19.9	23.6
	366	0.05	2	40.3	53.7	84.0	1.5
		0.85	32	37.0	49.1	73.3	22.4
		1.27	47	35.1	45.5	68.8	31.2
		2.65	97	28.8	35.0	56.0	56.3
$CaCl_2$	300	0.05	3	8.4	21.3	32.1	1.5
		0.45	24	7.7	17.1	26.7	10.9
		0.60	32	7.4	16.1	25.2	13.8
		0.89	47	6.2	13.9	21.9	17.4

[a] D_{cation} refers to D_{Na} or D_{Ca}.

DOI: 10.1021/acs.jpcc.5b10851
J. Phys. Chem. C 2016, 120, 1640−1649

Table 5. Comparison of Water Diffusion Coefficients (10^{-10} $m^2 \cdot s^{-1}$) in Sodium Smectite Interlayers from Experiment and MD Simulation at Room Temperature.[a]

sample	layer charge (e·unit cell^{-1})	method	water layers	D_w
montmorillonite	−0.750	MD[b]	1W	4.6
			2W	13.1
	−0.76	QENS[60]	1W	1−3
			2W	5−10
	−1.03	QENS[59]	2W	8.0
saponite	−0.8	QENS[16]	1W	3.8−8.0
			2W	5.7−12.1
fluorohectorite	−0.8	QENS[53,54]	1W	2.8
			2W	4.9−6.9[b]

[a]Experimental values were determined for diffusion parallel to the clay layers and were performed at either 298 or 300 K. [b]This work, 300 K.

water diffusion between interlayer regions and bulk solutions are discussed in more detail below, but we note here that interlayer D_w and D_{ion} values are significantly lower than in bulk solution or even more concentrated solutions. Diffusion coefficients at 0.05 M are in good agreement with published simulation results for bulk water[55] and NaCl(aq) at infinite dilution.[56] It is well-known that D_w predicted by the flexible SPC water model is larger than the experimental value of 23.5 × 10^{-10} $m^2 \cdot s^{-1}$.[57] Finally, we note that our simulation results for ion diffusion coefficients in bulk solution are in good agreement with the experimental values of 13.3 × 10^{-10} $m^2 \cdot s^{-1}$ (Na^+), 7.9 × 10^{-10} $m^2 \cdot s^{-1}$ (Ca^{2+}), and 20.3 × 10^{-10} $m^2 \cdot s^{-1}$ (Cl^-).[58]

Experimental values of water diffusion in Na-smectites are available from quasi-elastic neutron scattering (QENS) for comparison (Table 5). Both simulation and experiment reveal the dramatic increase in water diffusion between the 1W and 2W states, and both methods show that water diffusion in the 2W states is significantly reduced compared to bulk water (discussed below). Simulated D_w values for Na-montmorillonite are consistently larger than experiment, but for the 2W state of Ca-montmorillonite we note that the simulated value of D_w (8.6 × 10^{-10} $m^2 \cdot s^{-1}$) is slightly lower than the experimental value (12.0 × 10^{-10} $m^2 \cdot s^{-1}$).[59] For synthetic Na-saponite (−0.8 e·unit cell^{-1}) at 300 K, two D_w values for each hydration state were reported, depending on the QENS energy resolution.[16] Our simulated D_w value for the 1W state lies between the experimental values, while for the 2W state, the simulation value is slightly larger than the upper value of the reported range.

For synthetic Na-fluorohectorite (−0.8 e·unit cell^{-1}),[53,54] D_w values from QENS experiments are approximately half as large as our simulated montmorillonite results for both the 1W and 2W states. MD simulations of the fluorohectorite models also showed an overestimation of D_w values compared with experiment, although a definite explanation for this trend remains unclear.[54] Given the differences in clay structure and layer charge between the simulation model and the experimental samples, our simulated water diffusion coefficients compare favorably with the available experimental data.

Although experimental values for ion diffusion in clays are available from tracer diffusion or impedance spectroscopy, the use of compacted clay samples of varying water contents and porosities makes a quantitative comparison difficult. A range of experimental D_{ion} values at 298 K have been reported for Kunipia-F montmorillonite with similar layer charge characteristics as our simulation model: 0.1 × 10^{-10} −0.8 × 10^{-10} $m^2 \cdot s^{-1}$ (Na^+)[61] and 0.06 × 10^{-10}−0.2 × 10^{-10} $m^2 \cdot s^{-1}$ (Ca^{2+})[62] over a range of dry densities of 1.0−1.8 $Mg \cdot m^{-3}$. These values are slightly lower than our simulation results for high-charge montmorillonite, but the trend of $D_{Na} > D_{Ca}$ is consistent. For Na^+ diffusion in compacted MX-80 montmorillonite (layer charge −1.12 e·unit cell^{-1}) at 293 K, D_{ion} values of 0.54 × 10^{-10} $m^2 \cdot s^{-1}$ and 9.6 × 10^{-10} $m^2 \cdot s^{-1}$ have been reported at relative humidities of 30% (1W) and 90% (2W), respectively.[63] In comparison, our simulation results slightly overpredict the 1W value and underpredict the 2W value, but given the difference in clay sample (including layer charge), the comparison is reasonable.

Additional simulations were performed on high-charge Na-montmorillonite at higher temperatures to obtain activation energies of sodium and water diffusion. Arrhenius plots of sodium and water diffusion over the temperature range 300−366 K (Figure 2) show a consistent behavior. Reduced mobility as a result of extreme confinement results in small D values in the 1W state (interlayer width = 2.6 Å) relative to 2W (5.2 Å) and 3W (7.4 Å). The similarity of activation energy (E_{act}) values (Table 6) follow from the nearly identical Arrhenius plots. Such a narrow range of E_{act} values for sodium ions and water molecules across a range of hydration states is best explained by considering that any translational motion of interlayer species involves breaking of hydrogen bonds (H-bonds) as the initiation step. It is not surprising, therefore, that the E_{act} values in Table 6 are consistent with that of pure water at 298 K (16.9 $kJ \cdot mol^{-1}$) from QENS experiments[59] and the H-bond strength between two water molecules (20.5 $kJ \cdot mol^{-1}$).[64] Our water E_{act} values also compare well with those reported from QENS experiments of Na-montmorillonite.[59,65] The slight increase in sodium ion E_{act} at higher water content is not consistent with the expected trend of decreasing E_{act} with increasing water content,[61] but all three values are similar to the value in dilute aqueous solution (18.4 $kJ \cdot mol^{-1}$).[66] In MD simulations of Na-hectorite, Marry et al.[53] noted that diffusion coefficients and activation energies were sensitive to stacking of adjacent clay layers. Although we have made no attempt to simulate montmorillonites in different stacking arrangements, we have taken care to use random configurations of layer charge sites to avoid the influence of adjacent clay layers on our results.

A graphical comparison of D_{ion} and D_w values (Figures 3 and 4) reveals the consistency in diffusion behavior between bulk solution and clay interlayers. Error bars are not shown in the diffusion plots since the errors are sufficiently small (<0.65%). Molar ion concentrations in the bulk models are lower than the interlayer fluids, but the parts per million concentrations are similar (Tables 1−2). The presence of confining clay surfaces

DOI: 10.1021/acs.jpcc.5b10851
J. Phys. Chem. C 2016, 120, 1640−1649

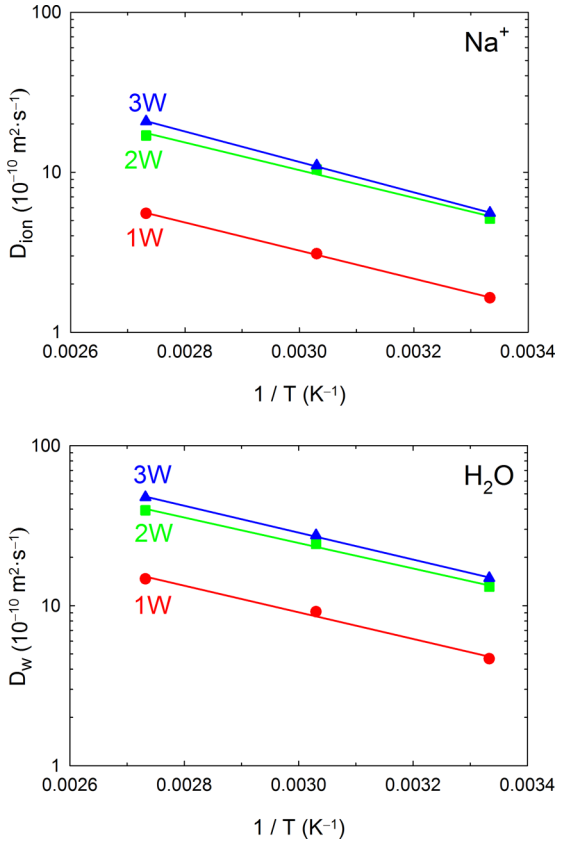

Figure 2. Arrhenius plots of sodium ion and water diffusion in montmorillonite interlayers (layer charge −0.750 *e*/u.c.).

Table 6. Activation Energies (kJ·mol^{-1}) for Sodium Ion and Water Diffusion in Montmorillonite Interlayers (−0.750 *e*/u.c.)

water layers	E_{act} (Na^+)	E_{act} (H_2O)
1W	16.8	15.9
2W	16.5	15.2
3W	18.2	16.1

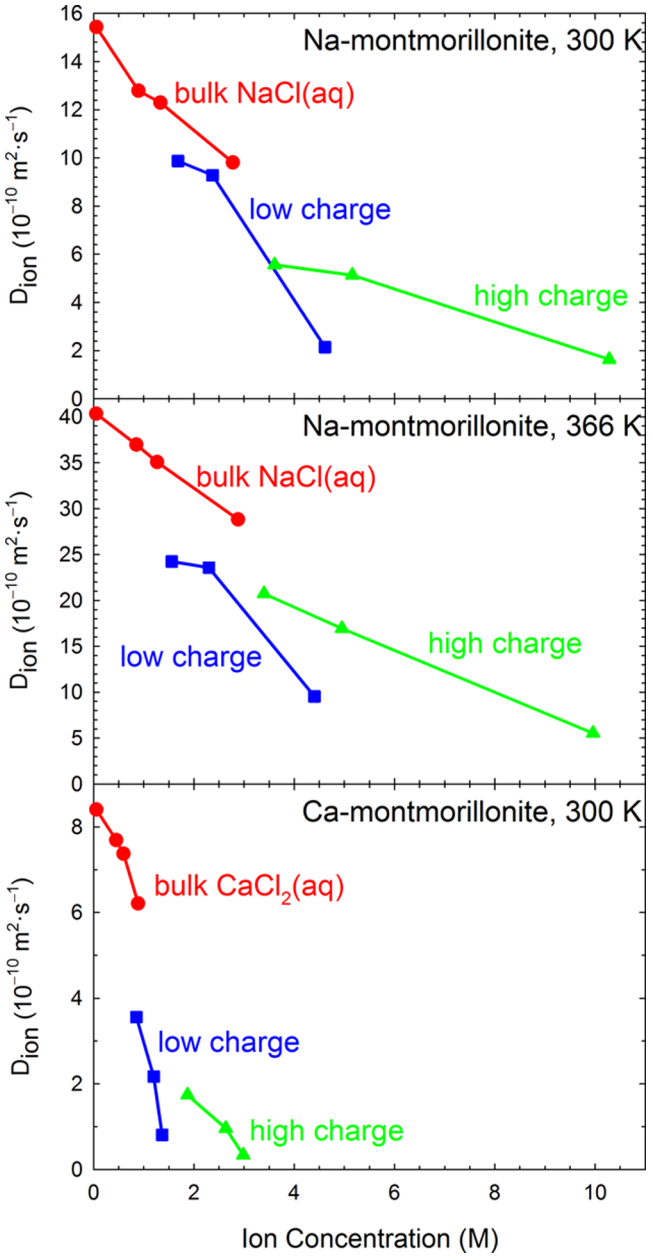

Figure 3. Ion diffusion coefficients vs concentration in Na- and Ca-montmorillonite interlayers and bulk NaCl(aq) and $CaCl_2$(aq) solutions at 300 K (Na and Ca) and 366 K (Na). Model systems consist of low-charge montmorillonite (−0.375 *e*·u.c.$^{-1}$, blue squares), high-charge montmorillonite (−0.75 *e*·u.c.$^{-1}$, green triangles), and bulk solutions (red circles).

reduces the accessible volume available to the interlayer fluid, resulting in much higher molar concentrations compared to the bulk solutions. A clear trend of decreasing diffusion coefficients with increasing electrolyte concentration is observed for the bulk solutions. The same trend holds for the interlayer fluids, and surprisingly the interlayer D values appear to extend the curves established by the bulk solution values. This feature is particularly apparent for Na-montmorillonite (both ion and water) but less obvious for Ca-montmorillonite due to the sharp decrease in diffusion with increasing concentration. In the case of low-charge Na- and Ca-montmorillonite, the interlayer ion concentrations in the 2W and 3W states lie within the range of the bulk solutions, and the D_w values nearly overlap. Interlayer ions are more strongly influenced by the charged clay surfaces, so the interlayer D_{ion} values are lower than their bulk solution counterparts.

The concentration-dependent diffusion behavior in clay interlayers suggests that these fluids behave as concentrated (neutral) aqueous solutions. Rather than adopt the common practice of comparing structural and dynamic properties of interlayer fluids with bulk water or dilute electrolyte solutions, Figures 3 and 4 suggest that a reference solution of equivalent cation concentration seems much more appropriate. Simulations of bulk solutions at higher molar concentrations were not attempted due to the significant ion pairing expected. These ion−water potentials[67,68] have not been validated for such concentrated solutions. The only evidence of ion pairing in the bulk solutions was seen in the 2.78 M NaCl solution. An examination of average radial distribution function data from this simulation at 300 K (data not shown) revealed a contact ion pair with a Na−Cl separation of 2.8 Å and a coordination number of 0.3. Approximately 30% of sodium ions were paired with chloride ions in this concentrated solution, which might reduce the mobility of each ion. However, as with the less concentrated solutions, D_{Cl} is greater than D_{Na} (Table 4), but

DOI: 10.1021/acs.jpcc.5b10851
J. Phys. Chem. C 2016, 120, 1640−1649

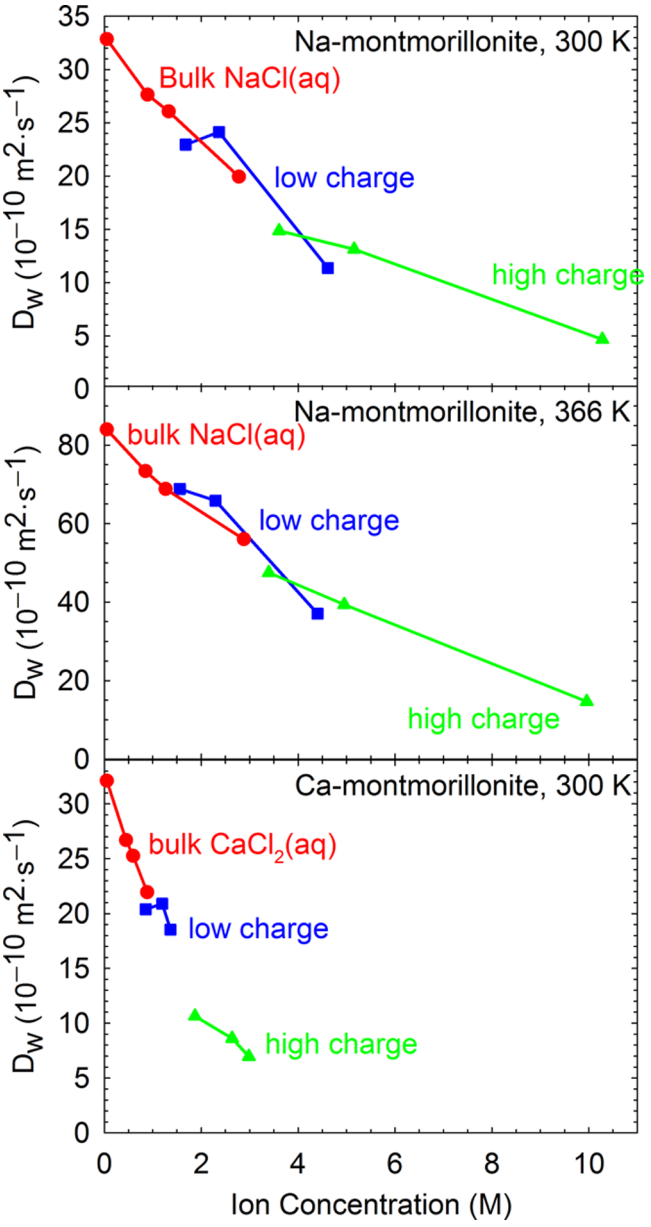

Figure 4. Water diffusion coefficients vs ion concentration in Na- and Ca-montmorillonite interlayers and bulk NaCl(aq) and $CaCl_2$(aq) solutions at 300 K (Na and Ca) and 366 K (Na). Model systems consist of low-charge montmorillonite (−0.375 e·u.c.$^{-1}$, blue squares), high-charge montmorillonite (−0.75 e·u.c.$^{-1}$, green triangles), and bulk solutions (red circles).

with ion pairing effects this difference is smaller at higher concentration. Ion pairing did not occur in the $CaCl_2$ solutions to an appreciable extent. Even for the most concentrated solution (0.89 M) at 300 K, the average Ca−Cl coordination number was only 0.03.

One helpful application of the diffusion data derived through from MD simulations is the determination of mass diffusion penetration depth δ ($=2\sqrt{Dt}$) which provides an approximate distance of mass diffusion transport for a given time.[69] Conversely, it can be used to estimate the time required for a diffusing species to transport a prescribed distance; for example, from a clay particle through its interlayer and into a coexisting aqueous phase. Assuming a clay grain is 2 μm in diameter (at the large end of the size distribution), it would take about 0.7 ms for Na^+ and just 0.2 ms for H_2O to diffuse outward from the middle of the clay grain, based on the diffusion data derived by MD simulations for the low-charge 1W montmorillonite at 300 K. It would require roughly one-third the corresponding time for both Na^+ (0.2 ms) and H_2O (0.07 ms) for a montmorillonite expanded to a 3W hydrate.

Electrical conductivities were calculated from D_{ion} values and are plotted as a function of TDS concentration in Figure 5. In the case of bulk solutions, TDS values include cations and chloride ions. The ppm scale is used to reflect ion concentration units more commonly seen in conductivity measurements. Solution concentrations and therefore volumes are required in the calculation of electrical conductivity (eq 3),

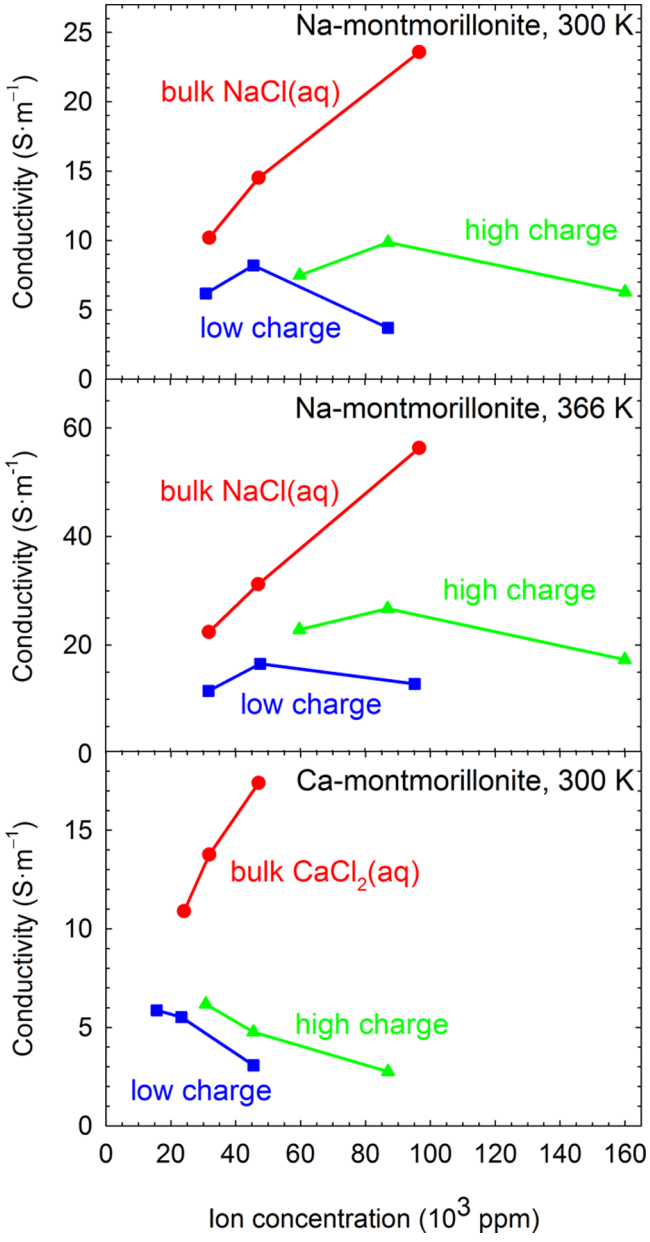

Figure 5. Electrical conductivity vs TDS concentration in Na- and Ca-montmorillonite interlayers and bulk NaCl(aq) and $CaCl_2$(aq) solutions at 300 K (Na and Ca) and 366 K (Na). Model systems consist of low-charge montmorillonite (−0.375 e·u.c.$^{-1}$, blue squares), high-charge montmorillonite (−0.75 e·u.c.$^{-1}$, green triangles), and bulk solutions (red circles).

DOI: 10.1021/acs.jpcc.5b10851
J. Phys. Chem. C 2016, 120, 1640−1649

so uncertainties in our calculation of fluid volumes could affect the resulting conductivity values. However, given the small uncertainties in average cell parameters (0.07 Å) combined with the small possible error in volume due to surface hexagonal cavities, we feel that uncertainties in our calculated conductivity values would have a minimal effect in the conductivity trends shown in Figure 5.

While the conductivity of NaCl and $CaCl_2$ solutions increases linearly with concentration over the ppm range relevant to clay interlayers, the conductivity of Na- and Ca-montmorillonite interlayers does not follow the same linear trend. Since the clay interlayers only contain cations and no chloride anions, interlayer conductivity generally decreases with increasing (cation) concentration, as seen in the ion diffusion trends (Figure 3). For bulk solutions, the contribution of diffusing cations and anions results in the opposite trend in observed conductivity values compared to diffusion values.

For Na-montmorillonite, conductivity increases between the 3W (less concentrated) and 2W (more concentrated) states, followed by a decrease in conductivity at the most concentrated 1W state. In Ca-montmorillonite, ionic strength effects result in decreasing conductivity as concentration increases. Additionally, the linear trend for bulk solutions allows for approximate bulk conductivity values to be determined for each ppm value in the interlayer fluids. Because electrical conductivity varies linearly with ion diffusion (eq 2), trends in the two properties are similar. One significant difference is seen in the conductivity trends at lower water content (higher ppm concentration). Rather than a linear trend of increasing σ with increasing ppm concentration, interlayer conductivities at the highest ion concentrations (1W) are similar to or lower than the 2W values. We also note that layer charge exerts less influence on conductivity than diffusion. Additionally, our simulated conductivity values for the 2W and 3W hydration states of high-charge Na-montmorillonite at 300 K (Figure 5a) compare favorably to the values obtained by Salles et al. using impedance spectroscopy on MX-80 Na-montmorillonite at 293 K.[63]

Plots of relative electrical conductivity (Figure 6) allow for a more direct comparison of interlayer conductivity between clays with different layer charge and exchangeable cation. Regardless of layer charge, relative conductivities for Na-montmorillonite at 300 K are nearly identical to the values at 366 K. This is an important finding for conductivity experiments in the field, where temperatures can vary widely. Plotting relative conductivity on a porosity scale, results for the commonly occurring 2W states can easily be compared. In this case, clays with reduced layer charge show a higher relative conductivity than clays with higher layer charge. This result follows directly from trends in ion diffusion (Figure 3) showing that ions diffuse faster in low\-charge interlayers.

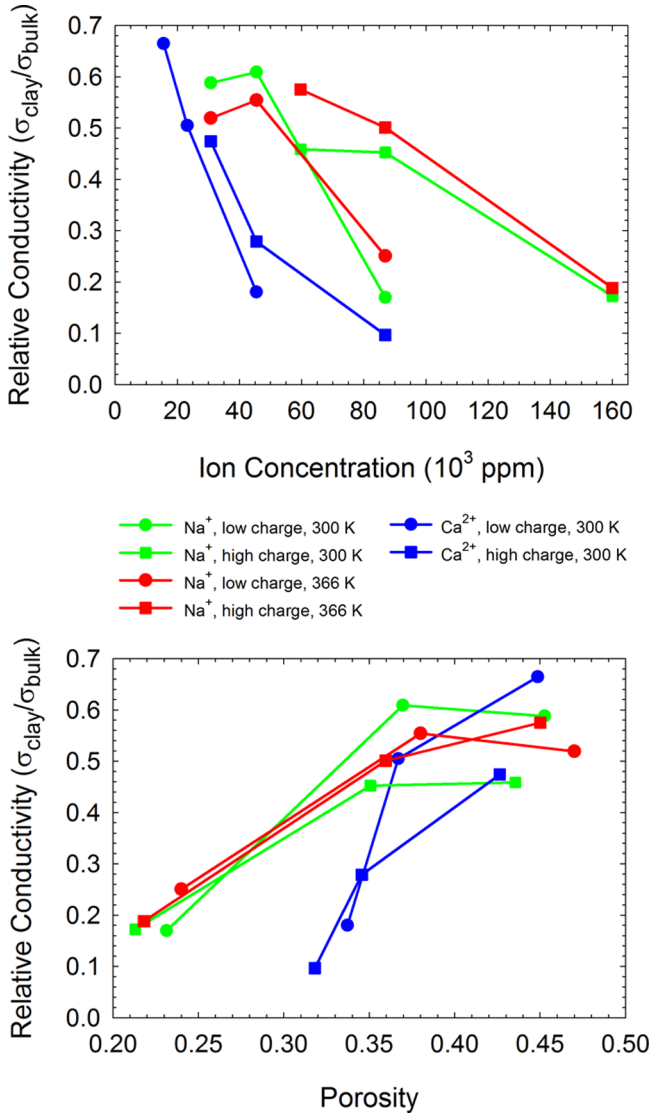

Figure 6. Relative electrical conductivity ($\sigma_{clay}/\sigma_{bulk}$) vs interlayer ion concentration (top) and interlayer porosity (bottom) for sodium (squares) and calcium (circles) counterions in low-charge (blue) and high-charge (green) montmorillonite. Here σ_{bulk} refers to the ion conductivity of a reference solution with the same TDS concentration as the interlayer fluid.

CONCLUSIONS

MD simulations have been used to investigate transport properties of ions and water in montmorillonite interlayers and corresponding bulk electrolyte solutions. By varying the layer charge (low and high charge), interlayer cation (Na^+ and Ca^{2+}), water content (1W − 3W states), and temperature (300 K − 366 K), we have developed a better understanding of some of the key factors governing interlayer transport in clays. Not surprisingly, reduced layer charge leads to a more hydrophobic interlayer environment with significantly faster diffusional motion compared to the high-charge models. Interlayer water content only plays a significant role in the 1W state of Na-montmorillonite, where some sodium ions are directly adsorbed to the siloxane surface and are less mobile. At higher water contents of Na-montmorillonite and for Ca-montmorillonite at all hydration states, additional water has very little effect on ion or water diffusion. In those cases, the interlayer cations are fully hydrated, and an Arrhenius analysis indicates that water and ion activation energies are similar to each other and to the hydrogen bond energy in water. Thus, we can conclude that hydrogen bond breaking is a key step in the diffusion of interlayer water or ions.

Although diffusion coefficients for interlayer water never approach that of pure water, our comparisons with bulk NaCl and $CaCl_2$ solutions show that the diffusion properties of interlayer fluids are analogous to bulk solutions of similar ion concentration. In fact, ion and water diffusion coefficients from both interlayer fluids and bulk solutions follow the same trend of decreasing diffusion coefficient with increasing ion concentration. In the cases where the interlayer ion

DOI: 10.1021/acs.jpcc.5b10851
J. Phys. Chem. C 2016, 120, 1640−1649

concentration is similar to that of a bulk solution, the diffusion coefficients are nearly identical.

Diffusion coefficients were converted to electrical conductivity values to provide insight into conductivity measurements at the laboratory or field scale. Comparing conductivities of interlayer fluids with bulk solutions based on a ppm scale of TDS, the confined interlayer fluids have much lower values than bulk solutions with similar ppm concentration. Finally, a comparison of relative electrical conductivity values for interlayer fluids reveals consistent behavior as a function of ion concentration or interlayer porosity, regardless of temperature, layer charge, or interlayer cation.

While diffusion coefficients from MD simulations of clay interlayers have often been carefully compared to high-quality experimental measurements using synchrotron techniques, our results suggest that a comparison of simulated and experimental conductivity measurements would yield additional insight into the dynamic behavior in clays.

AUTHOR INFORMATION

Notes

The authors declare no competing financial interest.

ACKNOWLEDGMENTS

Sandia National Laboratories is a multiprogram laboratory managed and operated by Sandia Corporation, a wholly owned subsidiary of Lockheed Martin Corporation, for the U.S. Department of Energy's National Nuclear Security Administration under contract DE-AC04-94AL85000. This work was funded by BP America, and BP management is thanked for permission to publish this work.

REFERENCES

(1) Blyth, A. R.; Frape, S. K.; Tullborg, E. L. A Review and Comparison of Fracture Mineral Investigations and Their Application to Radioactive Waste Disposal. *Appl. Geochem.* **2009**, *24*, 821−835.

(2) Kumpiene, J.; Lagerkvist, A.; Maurice, C. Stabilization of As, Cr, Cu, Pb, and Zn in Soil Using Amendments: A Review. *Waste Manage.* **2008**, *28*, 215−225.

(3) Nasser, A.; Mingelgrin, U. Mechanochemistry: A Review of Surface Reactions and Environmental Applications. *Appl. Clay Sci.* **2012**, *67*−*68*, 141−150.

(4) Shackelford, C. D.; Moore, S. M. Fickian Diffusion of Radionuclides for Engineered Containment Barriers: Diffusion Coefficients, Porosities, and Complicating Issues. *Eng. Geol.* **2013**, *152*, 133−147.

(5) Udeigwe, T. K.; Eze, P. N.; Teboh, J. M.; Stietiya, M. H. Application, Chemistry, and Environmental Implications of Contaminant-Immobilization Amendments on Agricultural Soil and Water Quality. *Environ. Int.* **2011**, *37*, 258−267.

(6) Yuan, P.; Liu, H. M.; Liu, D.; Tan, D. Y.; Yan, W. C.; He, H. P. Role of the Interlayer Space of Montmorillonite in Hydrocarbon Generation: An Experimental Study Based on High Temperature−Pressure Pyrolysis. *Appl. Clay Sci.* **2013**, *75*−*76*, 82−91.

(7) Altmann, S. 'Geo'chemical Research: A Key Building Block for Nuclear Waste Disposal Safety Cases. *J. Contam. Hydrol.* **2008**, *102*, 174−179.

(8) Dupray, F.; Francois, B.; Laloui, L. Analysis of the FEBEX Multi-Barrier System Including Thermoplasticity of Unsaturated Bentonite. *Int. J. Numer. Anal. Methods Geomech.* **2013**, *37*, 399−422.

(9) Fernandez, A. M.; Villar, M. V. Geochemical Behaviour of a Bentonite Barrier in the Laboratory after up to 8 Years of Heating and Hydration. *Appl. Geochem.* **2010**, *25*, 809−824.

(10) Marty, B.; Dewonck, S.; France-Lanord, C. Geochemical Evidence for Efficient Aquifer Isolation over Geological Timeframes. *Nature* **2003**, *425*, 55−58.

(11) Cuevas, J.; Ruiz, A. I.; de Soto, I. S.; Sevilla, T.; Procopio, J. R.; Da Silva, P.; Gismera, M. J.; Regadio, M.; Jimenez, N. S.; Rastrero, M. R.; Leguey, S. The Performance of Natural Clay as a Barrier to the Diffusion of Municipal Solid Waste Landfill Leachates. *J. Environ. Manage.* **2012**, *95*, S175−S181.

(12) Kang, J. B.; Shackelford, C. D. Membrane Behavior of Compacted Clay Liners. *J. Geotech. Geoenviron. Eng.* **2010**, *136*, 1368−1382.

(13) Rowe, R. K. Long-Term Performance of Contaminant Barrier Systems. *Geotechnique* **2005**, *55*, 631−677.

(14) Bourg, I. C.; Sposito, G. Connecting the Molecular Scale to the Continuum Scale for Diffusion Processes in Smectite-Rich Porous Media. *Environ. Sci. Technol.* **2010**, *44*, 2085−2091.

(15) Bourg, I. C.; Steefel, C. I. Molecular Dynamics Simulations of Water Structure and Diffusion in Silica Nanopores. *J. Phys. Chem. C* **2012**, *116*, 11556−11564.

(16) Michot, L. J.; Ferrage, E.; Jimenez-Ruiz, M.; Boehm, M.; Delville, A. Anisotropic Features of Water and Ion Dynamics in Synthetic Na- and Ca-Smectites with Tetrahedral Layer Charge. A Combined Quasielastic Neutron-Scattering and Molecular Dynamics Simulations Study. *J. Phys. Chem. C* **2012**, *116*, 16619−16633.

(17) Churakov, S. V. Mobility of Na and Cs on Montmorillonite Surface under Partially Saturated Conditions. *Environ. Sci. Technol.* **2013**, *47*, 9816−9823.

(18) Ferrage, E.; Lanson, B.; Sakharov, B. A.; Drits, V. A. Investigation of Smectite Hydration Properties by Modeling Experimental X-ray Diffraction Patterns: Part I. Montmorillonite Hydration Properties. *Am. Mineral.* **2005**, *90*, 1358−1374.

(19) Ferrage, E.; Sakharov, B. A.; Michot, L. J.; Delville, A.; Bauer, A.; Lanson, B.; Grangeon, S.; Frapper, G.; Jimenez-Ruiz, M.; Cuello, G. J. Hydration Properties and Interlayer Organization of Water and Ions in Synthetic Na-Smectite with Tetrahedral Layer Charge. Part 2. Toward a Precise Coupling between Molecular Simulations and Diffraction Data. *J. Phys. Chem. C* **2011**, *115*, 1867−1881.

(20) Cygan, R. T.; Liang, J.-J.; Kalinichev, A. G. Molecular Models of Hydroxide, Oxyhydroxide, and Clay Phases and the Development of a General Force Field. *J. Phys. Chem. B* **2004**, *108*, 1255−1266.

(21) Rotenberg, B.; Marry, V.; Vuilleumier, R.; Malikova, N.; Simon, C.; Turq, P. Water and Ions in Clays: Unraveling the Interlayer/Micropore Exchange Using Molecular Dynamics. *Geochim. Cosmochim. Acta* **2007**, *71*, 5089−5101.

(22) Rotenberg, B.; Morel, J.-P.; Marry, V.; Turq, P.; Morel-Desrosiers, N. On the Driving Force of Cation Exchange in Clays: Insights from Combined Microcalorimetry Experiments and Molecular Simulation. *Geochim. Cosmochim. Acta* **2009**, *73*, 4034−4044.

(23) Amarasinghe, P. M.; Anandarajah, A. Molecular Dynamic Study of the Swelling Behavior of Na-Montmorillonite. *Environ. Eng. Geosci.* **2013**, *19*, 173−183.

(24) Tambach, T. J.; Bolhuis, P. G.; Hensen, E. J. M.; Smit, B. Hysteresis in Clay Swelling Induced by Hydrogen Bonding: Accurate Prediction of Swelling States. *Langmuir* **2006**, *22*, 1223−1234.

(25) Tambach, T. J.; Hensen, E. J. M.; Smit, B. Molecular Simulations of Swelling Clay Minerals. *J. Phys. Chem. B* **2004**, *108*, 7586−7596.

(26) Nasreldin, H. A. Fluid Dynamics of Oil−Water−Sand Systems. *Adv. Chem. Ser.* **1992**, *231*, 171−217.

(27) Atekwana, E. A.; Atekwana, E.; Legall, F. D.; Krishnamurthy, R. V. Biodegradation and Mineral Weathering Controls on Bulk Electrical Conductivity in a Shallow Hydrocarbon Contaminated Aquifer. *J. Contam. Hydrol.* **2005**, *80*, 149−167.

(28) Mohammadi, A. H.; Martinez-Lopez, J. F.; Richon, D. Determination of Hydrate Stability Zone Using Electrical Conductivity Data of Salt Aqueous Solution. *Fluid Phase Equilib.* **2007**, *253*, 36−41.

(29) Kaufhold, S.; Grissemann, C.; Dohrmann, R.; Klinkenberg, M.; Decher, A. Comparison of Three Small-Scale Devices for the

DOI: 10.1021/acs.jpcc.5b10851
J. Phys. Chem. C 2016, 120, 1640−1649

Investigation of The Electrical Conductivity/Resistivity of Swelling and Other Clays. *Clays Clay Miner.* **2014**, *62*, 1−12.
(30) Liang, J. J.; Hawthorne, F. C.; Swainson, I. P. Triclinic Muscovite: X-ray Diffraction, Neutron Diffraction and Photo-Acoustic FTIR Spectroscopy. *Can. Mineral.* **1998**, *36*, 1017−1027.
(31) Greathouse, J. A.; Durkin, J. S.; Larentzos, J. P.; Cygan, R. T. Implementation of a Morse Potential to Model Hydroxyl Behavior in Layered Auminosilicates. *J. Chem. Phys.* **2009**, *130*, 134713.
(32) Chang, F.-R. C.; Skipper, N. T.; Sposito, G. Computer Simulation of Interlayer Molecular Structure in Sodium Montmorillonite Hydrates. *Langmuir* **1995**, *11*, 2734−2741.
(33) Brindley, G. W.; Brown, G. *Crystal Structures of Clay Minerals and Their X-Ray Identification*; Mineralogical Society, 1980.
(34) Greathouse, J. A.; Hart, D. B.; Bowers, G. M.; Kirkpatrick, R. J.; Cygan, R. T. Molecular Simulation of Structure and Diffusion at Smectite−Water Interfaces: Using Expanded Clay Interlayers as Model Nanopores. *J. Phys. Chem. C* **2015**, *119*, 17126−17136.
(35) Holmboe, M.; Bourg, I. C. Molecular Dynamics Simulations of Water and Sodium Diffusion in Smectite Interlayer Nanopores as a Function of Pore Size and Temperature. *J. Phys. Chem. C* **2014**, *118*, 1001−1013.
(36) Larentzos, J. P.; Greathouse, J. A.; Cygan, R. T. An ab Initio and Classical Molecular Dynamics Investigation of the Structural and Vibrational Properties of Talc and Pyrophyllite. *J. Phys. Chem. C* **2007**, *111*, 12752−12759.
(37) Morrow, C. P.; Yazaydin, A. O.; Krishnan, M.; Bowers, G. M.; Kalinichev, A. G.; Kirkpatrick, R. J. Structure, Energetics, and Dynamics of Smectite Clay Interlayer Hydration: Molecular Dynamics and Metadynamics Investigation of Na-Hectorite. *J. Phys. Chem. C* **2013**, *117*, 5172−5187.
(38) Ebrahimi, D.; Pellenq, R. J. M.; Whittle, A. J. Nanoscale Elastic Properties of Montmorillonite upon Water Adsorption. *Langmuir* **2012**, *28*, 16855−16863.
(39) Shahriyari, R.; Khosravi, A.; Ahmadzadeh, A. Nanoscale Simulation of Na-Montmorillonite Hydrate under Basin Conditions, Application of CLAYFF Force Field in Parallel GCMC. *Mol. Phys.* **2013**, *111*, 3156−3167.
(40) Greathouse, J. A.; Cygan, R. T. Molecular Dynamics Simulation of Uranyl(VI) Adsorption Equilibria onto an External Montmorillonite Surface. *Phys. Chem. Chem. Phys.* **2005**, *7*, 3580−3586.
(41) Greathouse, J. A.; Cygan, R. T. Water Structure and Aqueous Uranyl(VI) Adsorption Equilibria onto External Surfaces of Beidellite, Montmorillonite, and Pyrophyllite: Results from Molecular Simulations. *Environ. Sci. Technol.* **2006**, *40*, 3865−3871.
(42) Wang, J. W.; Kalinichev, A. G.; Kirkpatrick, R. J. Effects of Substrate Structure and Composition on the Structure, Dynamics, and Energetics of Water at Mineral Surfaces: A Molecular Dynamics Modeling Study. *Geochim. Cosmochim. Acta* **2006**, *70*, 562−582.
(43) Vasconcelos, I. F.; Bunker, B. A.; Cygan, R. T. Molecular Dynamics Modeling of Ion Adsorption to the Basal Surfaces of Kaolinite. *J. Phys. Chem. C* **2007**, *111*, 6753−6762.
(44) Liu, X. D.; Lu, X. C. A Thermodynamic Understanding of Clay-Swelling Inhibition by Potassium Ions. *Angew. Chem., Int. Ed.* **2006**, *45*, 6300−6303.
(45) Bourg, I. C.; Sposito, G. Molecular Dynamics Simulations of the Electrical Double Layer on Smectite Surfaces Contacting Concentrated Mixed Electrolyte ($NaCl-CaCl_2$) Solutions. *J. Colloid Interface Sci.* **2011**, *360*, 701−715.
(46) Teleman, O.; Jonsson, B.; Engstrom, S. A Molecular Dynamics Simulation of a Water Model with Intramolecular Degrees of Freedom. *Mol. Phys.* **1987**, *60*, 193−203.
(47) Plimpton, S. J. Fast Parallel Algorithms for Short-Range Molecular Dynamics. *J. Comput. Phys.* **1995**, *117*, 1−19.
(48) Plimpton, S. J.; Pollock, R.; Stevens, M. Particle-Mesh Ewald and rRESPA for Parallel Molecular Dynamics Simulations; Eighth SIAM Conference on Parallel Processing for Scientific Computing, 1997.
(49) Frenkel, D.; Smit, B. *Understanding Molecular Simulation: From Algorithms to Applications*, 2nd ed.; Academic Press: San Diego, CA, 2002.
(50) Zhang, L. H.; Lu, X. C.; Liu, X. D.; Zhou, J. H.; Zhou, H. Q. Hydration and Mobility of Inter layer Ions of (Na_x, Ca_y)-Montmorillonite: A Molecular Dynamics Study. *J. Phys. Chem. C* **2014**, *118*, 29811−29821.
(51) Bockris, J. O. M.; Reddy, A. K. N. *Modern Electrochemistry 1: Ionics*, 2nd ed.; Plenum Press: New York, 1998.
(52) Malikova, N.; Marry, V.; Dufreche, J. F.; Simon, C.; Turq, P.; Giffaut, E. Temperature Effect in a Montmorillonite Clay at Low Hydration-Microscopic Simulation. *Mol. Phys.* **2004**, *102*, 1965−1977.
(53) Marry, V.; Dubois, E.; Malikova, N.; Durand-Vidal, S.; Longeville, S.; Breu, J. Water Dynamics in Hectorite Clays: Infuence of Temperature Studied by Coupling Neutron Spin Echo and Molecular Dynamics. *Environ. Sci. Technol.* **2011**, *45*, 2850−2855.
(54) Marry, V.; Dubois, E.; Malikova, N.; Breu, J.; Haussler, W. Anisotropy of Water Dynamics in Clays: Insights from Molecular Simulations for Experimental QENS Analysis. *J. Phys. Chem. C* **2013**, *117*, 15106−15115.
(55) Wallqvist, A. T.; Teleman, O. O. Properties of Flexibile Water Molecules. *Mol. Phys.* **1991**, *74*, 515−533.
(56) Guardia, E.; Rey, R.; Padro, J. A. Na^+-Na^+ and Cl^-Cl^- Ion-Pairs in Water: Mean Force Potentials by Constrained Molecular Dynamics. *J. Chem. Phys.* **1991**, *95*, 2823−2831.
(57) Krynicki, K.; Green, C. D.; Sawyer, D. W. Pressure and Temperature Dependence of Self-Diffusion in Water. *Faraday Discuss. Chem. Soc.* **1978**, *66*, 199−208.
(58) *CRC Handbook of Chemistry and Physics*, 71st ed.; Lide, D. R., Ed.; CRC Press: Boca Raton, FL, 1990.
(59) Gates, W. P.; Bordallo, H. N.; Aldridge, L. P.; Seydel, T.; Jacobsen, H.; Marry, V.; Churchman, G. J. Neutron Time-of-Flight Quantification of Water Desorption Isotherms of Montmorillonite. *J. Phys. Chem. C* **2012**, *116*, 5558−5570.
(60) Malikova, N.; Cadene, A.; Marry, V.; Dubois, E.; Turq, P. Diffusion of Water in Clays on the Microscopic Scale: Modeling and Experiment. *J. Phys. Chem. B* **2006**, *110*, 3206−3214.
(61) Kozaki, T.; Fujishima, A.; Sato, S.; Ohashi, H. Self-Diffusion of Sodium Ions in Compacted Sodium Montmorillonite. *Nucl. Technol.* **1998**, *121*, 63−69.
(62) Kozaki, T.; Adachi, Y.; Inada, K.; Sato, S.; Ohashi, H. Diffusion Behavior of Ca2+ Ions in Compacted Na-Montmorillonite. *MRS Symp. Proc.* **2001**, *663*, 629−638.
(63) Salles, F.; Douillard, J. M.; Bildstein, O.; El Ghazi, S.; Prelot, B.; Zajac, J.; Van Damme, H. Diffusion of Interlayer Cations in Swelling Clays as a Function of Water Content: Case of Montmorillonites Saturated with Alkali Cations. *J. Phys. Chem. C* **2015**, *119*, 10370−10378.
(64) Feyereisen, M. W.; Feller, D.; Dixon, D. A. Hydrogen Bond Energy of the Water Dimer. *J. Phys. Chem.* **1996**, *100*, 2993−2997.
(65) Sánchez, F. t. G. l.; Gimmi, T.; Jurányi, F.; Loon, L. V.; Diamond, L. W. Linking the Diffusion of Water in Compacted Clays at Two Different Time Scales: Tracer Through-Diffusion and Quasielastic Neutron Scattering. *Environ. Sci. Technol.* **2009**, *43*, 3487−3493.
(66) Parsons, R. *Handbook of Electrochemical Constants*; Butterworths Scientific Publications: London, 1959.
(67) Smith, D. R.; Dang, L. X. Computer Simulations of NaCl Association in Polarizable Water. *J. Chem. Phys.* **1994**, *100*, 3757−3766.
(68) Koneshan, S.; Rasaiah, J. C.; Lynden-Bell, R. M.; Lee, S. H. Solvent Structure, Dynamics, and Ion Mobility in Aqueous Solutions at 25 Degrees C. *J. Phys. Chem. B* **1998**, *102*, 4193−4204.
(69) Crank, J. *The Mathematics of Diffusion*; Oxford University Press: London, 1975.

DOI: 10.1021/acs.jpcc.5b10851
J. Phys. Chem. C 2016, 120, 1640−1649